Available online at www.sciencedirect.com
SCIENCE DIRECT®
Pergamon
Acta Materialia 51 (2003) 3927–3938
Acta MATERIALIA
www.actamat-journals.com

In-situ study of pearlite nucleation and growth during isothermal austenite decomposition in nearly eutectoid steel

S.E. Offerman [a,b,*], L.J.G.W. van Wilderen [a,b], N.H. van Dijk [a], J. Sietsma [b], M.Th. Rekveldt [a], S. van der Zwaag [b, 1]

[a] *Interfaculty Reactor Institute, Delft University of Technology, Mekelweg 15, 2629 JB Delft, The Netherlands*
[b] *Laboratory of Materials Science, Delft University of Technology, Rotterdamseweg 137, 2628 AL Delft, The Netherlands*

Received 23 January 2003; received in revised form 10 April 2003; accepted 14 April 2003

Abstract

The evolution of the microstructure during the isothermal austenite/pearlite transformation in a nearly eutectoid steel was studied by the three-dimensional neutron depolarization technique, which simultaneously provides information about the pearlite fraction, the average pearlite colony size, and the spatial distribution of the pearlite colonies during the transformation. The in-situ measurements show that the pearlite nucleation rate increases linearly with time with a temperature-dependent slope. The in-situ measured average pearlite growth rate is accurately described by the Zener-Hillert theory, which assumes that volume diffusion of carbon is the rate-controlling mechanism. The measured overall transformation rate deviates from the predictions of the theory developed by Kolmogorov, Johnson, Mehl, and Avrami.

Keywords: Pearlitic steels; Phase transformation kinetics; Neutron depolarization

1. Introduction

Pearlite is a common constituent of a wide variety of steels and provides a substantial contribution to the strength. A pearlite colony consists of two interpenetrating single crystals of ferrite and cementite (Fe_3C), which are primarily ordered as alternating plates. Pearlite that consists of fine plates is harder and stronger than pearlite that consists of coarse plates. This morphology of pearlite is largely determined by the evolution of the austenite/pearlite phase transformation during the production process. Control of the pearlite phase transformation kinetics is thus of vital importance for the production of tailor-made steels.

Despite the large variety of austenite/pearlite phase transformation models that have been proposed and the experiments that have been performed to test them in the past 60 years, the kinetics of this transformation is still not completely understood. The reason why the pearlite nucleation mechanism is still not fully understood, lies in the

* Corresponding author. Tel.: +31-15-278-5630; fax: +31-15-278-8303.
E-mail address: S.E.Offerman@iri.tudelft.nl (S.E. Offerman).
[1] Present address: Faculty of Aerospace Engineering, Delft University of Technology, Kluyverweg 1, 2629 HS Delft, The Netherlands

1359-6454/03/$30.00
doi:10.1016/S1359-6454(03)00217-9

experimental difficulty to measure nucleation phenomena and in particular the nucleation of pearlite. The nucleation mechanism of pearlite involves the formation of two crystallographic phases. In hypo-eutectoid steels the pro-eutectoid ferrite nucleates first and continues to grow with the same crystallographic orientation during the pearlite formation as part of a pearlite colony [1,2]. In this case the cementite nucleation is the rate-limiting step in the formation of pearlite. In hyper-eutectoid steels the roles of ferrite and cementite are reversed and in perfectly eutectoid steel the pearlite nucleation is assumed to take place at the austenite grain corners, edges, and boundaries. However, the exact nature of the pearlite nucleation mechanism is still under debate.

Another important and continuing subject of debate is the rate-controlling mechanism for the growth of pearlite. There are two different theories proposed for the growth of pearlite. The Zener-Hillert theory assumes that the volume diffusion of carbon in the austenite, ahead of the advancing pearlite, is the rate-controlling mechanism [3,4]. The Hillert theory on the other hand assumes that grain boundary diffusion of the carbon atoms is the rate-controlling mechanism [5]. Several experimental studies were performed over the last decades in order to measure the pearlite growth rate and determine the rate-controlling mechanism. Both volume [6–9] and grain boundary diffusion [10] were claimed to be the rate-controlling mechanism, as well as more complex mechanisms [11].

The theory developed by Kolmogorov, Johnson, Mehl, and Avrami [12–16], also known as the KJMA theory, predicts the overall transformation rate on the basis of nucleation and growth rates. The KJMA-theory is one of the oldest and most widely used models to describe the pearlite phase transformation kinetics. This concept still forms the basis of many of the current phase transformation models.

The pearlite nucleation and growth rates have so far been determined from ex-situ optical and electron microscopy measurements, in which a series of steel specimens is annealed for increasing times at a particular transformation temperature. The high-temperature microstructure is frozen in at several stages of the transformation by quenching the specimen to room temperature. At each stage the largest pearlite colony size is determined, which is a measure for the pearlite growth rate. This method has two drawbacks. The first drawback is that it only gives an estimate of the pearlite growth rate if the largest pearlite colony can be related to the first pearlite colony that nucleated. The second drawback is that the method only reflects the highest observed growth rate.

These drawbacks can be avoided by using the three-dimensional Neutron Depolarization (3DND) technique [17,18], which has created the opportunity to study phase transformations in-situ in the bulk of steel. The 3DND technique provides a unique insight into the formation of the microstructure as it probes the volume fraction of the magnetic phase, the mean magnetic particle size, and the spatial distribution of the forming ferromagnetic phase in the paramagnetic (austenite) matrix [19]. The technique is capable of determining these three parameters in-situ and simultaneously, which makes it a powerful tool for the study of phase transformations in the bulk of ferromagnetic materials.

The aim of this research is to measure in-situ the pearlite fraction, the average pearlite colony size, and the spatial distribution as a function of the isothermal transformation time. This gives information about the nucleation rate, the rate-controlling mechanism for the growth of pearlite, and the validity of the KJMA theory for the prediction of the overall austenite/pearlite transformation rate. The present paper is related to two previous papers on the austenite/pearlite transformation in the same steel [20,21], which reported on the relation between the magnetic domain structure and the microstructure, and gave a comparison with the results of additional dilatometry experiments.

2. Pearlite transformation kinetics

2.1. Nucleation

The nucleation rate of the newly formed phase during a phase transformation is described by the classical nucleation theory [22], in which the time dependent nucleation rate $\dot{N}$ is expressed as

$$\dot{N} = N_n \beta^* Z \exp\left(-\frac{\Delta G^*}{k_B T}\right)\exp\left(-\frac{\tau}{t}\right), \quad (1)$$

where N_n is the number of potential nucleation sites, Z is the Zeldovich non-equilibrium factor, $k_B = 1.38 \times 10^{-23}$ J/K is the Boltzmann constant, and T the absolute temperature. The rate at which the iron atoms are added onto the critical nucleus is taken into account by the frequency factor β^*. The time τ represents the incubation time and t is the isothermal transformation time. The time-independent part of this equation is the steady state nucleation rate. The energy barrier that has to be overcome in order to form a critical nucleus is referred to as the activation energy for nucleation ΔG^*, which can in general be written as

$$\Delta G^* = \Psi / \Delta g_V^2. \quad (2)$$

The driving force for nucleation is the decrease in Gibbs free energy per unit volume of the system Δg_V during the phase transformation, which depends on the chemical composition and the temperature. The creation of a new nucleus requires energy due to the formation of an interface between the nucleus and the original phase. However, in the case that the nucleus is formed at a grain boundary the removal of incoherent austenite/austenite grain boundaries releases energy that can be used for the creation of a new interface. The balance between the energy that is required for the formation of a new interface and the energy that is released due to the removal of the old interface is represented by the factor Ψ. It is the uncertainty in Ψ which makes predictions of the nucleation rate very difficult.

2.2. Growth

Nucleation is followed by the growth of pearlite colonies. In the Zener-Hillert model [3,4], which assumes that volume diffusion of carbon is the rate-controlling mechanism for the growth of pearlite, the growth rate G_V is given by

$$G_V = \frac{D^\gamma_{C,V}}{k_V} \frac{\lambda^2}{\lambda^\alpha \lambda^\theta} \frac{C^{\gamma\alpha}_{eq} - C^{\gamma\theta}_{eq}}{C^\theta_{eq} - C^\alpha_{eq}} \frac{1}{\lambda}\left(1 - \frac{\lambda_c}{\lambda}\right), \quad (3)$$

where k_V is a geometrical constant related to the volume diffusion mechanism, $D^\gamma_{C,V}$ is the volume diffusion coefficient of carbon in austenite, and λ^α and λ^θ are the lamella thickness of the ferrite and cementite, respectively. The pearlite lamellar spacing amounts to $\lambda = \lambda^\alpha + \lambda^\theta$. $C^{\gamma\alpha}_{eq}$ and $C^{\gamma\theta}_{eq}$ are the equilibrium carbon concentrations in the austenite in contact with ferrite and cementite, respectively. C^α_{eq} and C^θ_{eq} are the equilibrium carbon concentrations in ferrite and cementite, respectively. The critical (theoretical minimum) spacing λ_c is given by

$$\lambda_c = \frac{2\gamma^{\alpha\theta} T_{A1}}{\Delta T} \frac{V_m}{\Delta H_m}, \quad (4)$$

where $\gamma^{\alpha\theta} = 0.94$ J/m^2 [23] is the interfacial free energy of the ferrite/cementite interface in the pearlite, T_{A1} (= 995 K for the studied steel) is the austenite/pearlite equilibrium transition temperature, $\Delta T = T_{A1} - T$ is the undercooling, ΔH_m = 4.3 kJ/mol [23] is the change in molar enthalpy, and $V_m = 7.1 \times 10^{-6}$ m^3/mol the molar volume. The volume diffusion coefficient of carbon in austenite $D^\gamma_{C,V}$ depends on the temperature and the nominal carbon concentration and can be described by [24]

$$D^\gamma_{C,V} = 4.53 \times 10^{-7}\left(1 + Y_C(1 - Y_C)\frac{8339.9}{T}\right) \times \exp\left\{-\left(\frac{1}{T} - 2.221 \times 10^{-4}\right)(17767 - 26436 Y_C)\right\}, \quad (5)$$

where $D^\gamma_{C,V}$ is in m^2/s and the temperature T in K. The site fraction Y_C of carbon on the interstitial sub-lattice is given by

$$Y_C = \frac{x_C}{1 - x_C}, \quad (6)$$

where x_C (= 0.0323 for the studied steel) is the overall atom fraction of carbon in the alloy.

In the Hillert model [5], which assumes that grain boundary diffusion of carbon is the rate-controlling mechanism for the growth of pearlite, the growth rate G_{GB} is given by:

$$G_{GB} = 12 k_{GB} D^\gamma_{C,GB} \delta \frac{\lambda^2}{\lambda^\alpha \lambda^\theta} \frac{C^{\gamma\alpha}_{eq} - C^{\gamma\theta}_{eq}}{C^\theta_{eq} - C^\alpha_{eq}} \frac{1}{\lambda^2} \left(1 - \frac{\lambda_c}{\lambda}\right), \quad (7)$$

where k_{GB} is the ratio of carbon concentration in the bulk of the austenite and the grain boundary and δ is the thickness of the boundary. The grain boundary diffusion coefficient of the carbon atoms $D^{\gamma}_{C,GB}$ can be estimated by assuming that the activation energy is half that of the activation energy for volume diffusion [25]. In the present case the argument of the exponential factor in Eq. (5) is multiplied by 0.5.

For the eutectoid composition $C^{\theta}_{eq} = 6.67$ wt.%, $C^{\alpha}_{eq} \approx 0.02$ wt.%, $\frac{\lambda^{\alpha}}{\lambda^{\theta}} \approx 7$, and $k_V = 0.72$ [4]. Further, we can assume that $C^{\gamma\theta}_{eq} - C^{\gamma\alpha}_{eq} \propto \Delta T$, and $\lambda \propto \Delta T^{-1}$ [26]. As a consequence the two different theories, represented by Eqs. (3) and (7), can be rewritten in the following form:

$$G_X = c_X D^{\gamma}_{C,X} (\Delta T)^{\beta}, \tag{8}$$

where the subscript X equals V or GB, which represents the volume or grain boundary diffusion theory, respectively. c_X is a constant, which is different for volume or grain boundary diffusion of carbon. The exponent β expresses the main difference between the two theories. For volume diffusion $\beta = 2$ and for grain boundary diffusion $\beta = 3$. Hence, the rate determining mechanism for the growth of pearlite can be determined from the exponent β.

2.3. Overall transformation

The overall pearlite transformation rate can be described by the KJMA theory, which predicts the fraction f of the formed phase as a function of the isothermal transformation time t as

$$f(t) = 1 - \exp\left(-k_g G^d \int_0^t \dot{N}_u(t')(t-t')^d dt' \right), \tag{9}$$

where G is a constant growth rate, d the dimensionality of the growth and k_g a constant, which depends on the geometry of the particle, e.g. $k_g = 4\pi/3$ for spherical particles ($d = 3$). The nucleation rate $\dot{N}_u$ is defined as the number of nuclei per unit untransformed volume per unit time. It is assumed that the nuclei are randomly distributed. The integration parameter t' can be interpreted as the time at which nucleation of grains took place.

Within the KJMA theory it is usually assumed that the nucleation rate is constant or that there is a fixed number of pre-existing nuclei throughout the transformation. However, Cahn [27] showed that when the nucleation rate, per unit untransformed volume, increases with time according to

$$\dot{N}_u(t) = k_u t^m, \tag{10}$$

where k_u and m are constants, the KJMA equation becomes

$$f(t) = 1 - \exp\left(-\frac{8\pi m!}{(d+m+1)!} k_u G^3 t^{m+4} \right), \tag{11}$$

for spherical particles that grow at a constant rate.

3. Three-dimensional neutron depolarization

The transmission of a monochromatic polarized neutron beam through the sample is characterized by the depolarization matrix $\boldsymbol{D}$ according to $\boldsymbol{P}' = \boldsymbol{D}\cdot\boldsymbol{P}$, where $\boldsymbol{P}$ and $\boldsymbol{P}'$ are the polarization vectors before and after transmission, respectively. The rotation of the polarization vector is a measure for the magnetic volume fraction and the degree of depolarization is a measure for the average magnetic domain size.

The rotation φ of the polarization vector is, in an eutectoid steel, related to the volume pearlite fraction f_p via

$$\varphi = \eta L c^{1/2} < \boldsymbol{B} >, \tag{12}$$

where L is the thickness of the sample, $c = 2.15 \times 10^{29}\ \lambda^2\ T^{-2} m^{-4}$, and $\lambda = 0.124(1)$ nm the neutron wavelength. The shape factor which accounts for the effect of stray fields

$$\eta = (1 - f_p)\eta^P + f_p \eta^M \tag{13}$$

is determined by a microscopic shape factor $\eta^P = 0.5$ for microscopic spherically shaped particles and a macroscopic shape factor $\eta^M = 0.905$ for our plate-like sample [28]. The average magnetic induction inside the sample is given by

$$< \boldsymbol{B} > \ = f_p < m_z > \mu_0 M^p_s, \tag{14}$$

where $<m_z>$ is the average reduced magnetization in the direction of the applied magnetic field (5.16

mT) along the long axis of the sample. The saturation magnetization of pearlite M_s^p can be calculated from the saturation magnetization of ferrite M_s^α [29] multiplied by the equilibrium volume fraction of ferrite f_α inside a pearlite colony. For the studied steel f_α is evaluated with the thermodynamic database MTDATA® and determined to be 0.90. During the experiment the temperature was higher than the Curie temperature of cementite, but was lower than the Curie Temperature of ferrite.

The depolarization of the polarized neutron beam, described by det($\boldsymbol{D}$), is caused by local variations in the magnetic induction $<(\Delta \boldsymbol{B})^2>$ inside the sample, and can be characterized for spherical particles by

$$\det(\boldsymbol{D}) = \exp\{-2cL\delta < (\Delta \boldsymbol{B})^2 > \}. \quad (15)$$

The average magnetic particle radius δ can be evaluated from the experimentally determined depolarization matrix $\boldsymbol{D}$ and model equations for $<(\Delta \boldsymbol{B})^2>$, which depends on f_p [18,19]. The measured depolarization can be written as $\det(\boldsymbol{D}) = D_\perp^2 D_{//}$, where $D_\perp$ and $D_{//}$ are the elements of the depolarization matrix $\boldsymbol{D}$ perpendicular and parallel to the applied magnetic field, respectively.

The polarized neutron beam probes the magnetic correlation length over which the local magnetic induction is oriented in the same direction, which means that δ represents the average distance over which the ferrite plates within a pearlite colony are more or less parallel [21]. In this paper it is assumed that the volume of a pearlite colony can be approximated by the volume in which the ferrite and cementite plates are more or less parallel. To a first approximation this assumption is valid, however from a crystallographic point of view a pearlite colony can be larger.

In the case that the magnetic particles are not randomly distributed over the sample, an extra depolarization of the polarized neutron beam will arise, which is not related to the magnetic domain size. This extra depolarization will affect all the elements of the depolarization matrix that are perpendicular to the applied magnetic field, while the component that is parallel to the magnetic field remains unaffected. In order to separate the contribution of the average magnetic domain size and the clustering (non-random spatial distribution) of particles to the depolarization, a cluster factor D_c is introduced:

$$D_c = \int_0^\infty f(N)\cos[(N-\langle N\rangle)\varphi_p]\mathrm{d}N, \quad (16)$$

where $f(N)$ is the normalized spatial distribution function of the number of particles N along a neutron path, $<N>$ is the average number of particles along the neutron path, and φ_p is the average rotation per domain [30]. The cluster factor is a measure for the degree of cluster formation in the specimen. It was shown [21] that the cluster factor can be deduced under certain conditions from the experiment according to

$$D_c = D_\perp \exp\left[-\frac{\ln(D_{//})}{\alpha_f}\right] \quad (17)$$

where, α_f represents the ratio $\ln(D_{//})/\ln(D_\perp)$ at the end of the transformation. In order to calculate the average magnetic domain size, the measured perpendicular component $D_\perp$ is multiplied by a factor $1/D_c$ [21]. The rotation φ of the polarization vector is not influenced by the manner in which the magnetic domains are distributed.

4. Experiment

The composition of the studied nearly eutectoid steel (in wt.%) is 0.715 C, 0.611 Mn, 0.266 Cr, 0.347 Si, 0.012 P, 0.03 S, 0.094 Ni, 0.235 Cu, 0.021 Mo, 0.025 Sn, and the rest is Fe. The austenite/pearlite phase transformation kinetics was studied by neutron depolarization and optical microscopy. The sample for the 3DND-experiments with dimensions $100 \times 15 \times 0.4$ mm^3 is coated with a nickel layer of approximately 15 μm thickness to avoid decarburization. The sample was annealed at 1173 K for 0.5 h in a nitrogen atmosphere, subsequently cooled with 20 K/s to 943 K, and held until the transformation was finished. This temperature cycle was repeated with the same sample for transformation temperatures of 948 and 953 K in order to study the influence of the degree of undercooling on the transformation kinetics. The 3DND measurements have been performed at the PANDA instrument at the nuclear reactor of the Interfaculty Reactor Institute.

Four cylindrical samples were prepared with a diameter of 5 mm and a length of 10 mm for examination with the optical microscope. The samples were annealed at 1173 K for 0.5 h under a vacuum of 10^{-4} mbar, cooled with 20 K/s to 953 K, held for either 50, 100, 150, or 200 s, and subsequently quenched to room temperature to freeze in the high-temperature microstructure.

5. Results

Fig. 1 shows the optical microscopy images of the microstructure at different stages of the isothermal austenite/pearlite phase transformation at $T = 953$ K ($\Delta T = 42$ K). When the transformation has proceeded for 50 s, the microstructure consists of individual pearlite colonies. After 100 s, also a few large clusters of pearlite colonies are observed besides the individual pearlite colonies. After 150 s more large clusters are formed, while individual pearlite colonies are still present. After 200 s the pearlite colonies have formed an interconnecting network, which encloses a number of untransformed austenite grains.

The corresponding 3DND measurements during the isothermal transformation at 953 K are presented in Fig. 2. Similar results were obtained for the isothermal transformations at 948 and 943 K. Fig. 2(a) shows that after approximately 300 s the rotation of the polarization vector φ reaches its final value, which indicates that the transformation is finished. Fig. 2(b) shows the components of the depolarization matrix D, which are perpendicular, $D_{\perp}$, and parallel, $D_{//}$, to the applied magnetic field, as a function of the transformation time. Around 150 s $D_{\perp}$ has a minimum, which is not present in $D_{//}$. From an earlier treatment of the data [21] we concluded that the magnetic domains are not randomly distributed during part of the transformation. The cluster factor D_c is obtained from Eq. (17) and α_f is determined to be 1.4.

The cluster factor D_c contains information about the cluster formation of pearlite colonies during the austenite/pearlite transformation, since it represents the spatial distribution of the magnetic domains in the sample. For a random distribution D_c equals one. As shown in Fig. 2(c) the factor D_c continuously decreases during the first stage of the transformation until it reaches a minimum half way the transformation. This indicates that the micro-

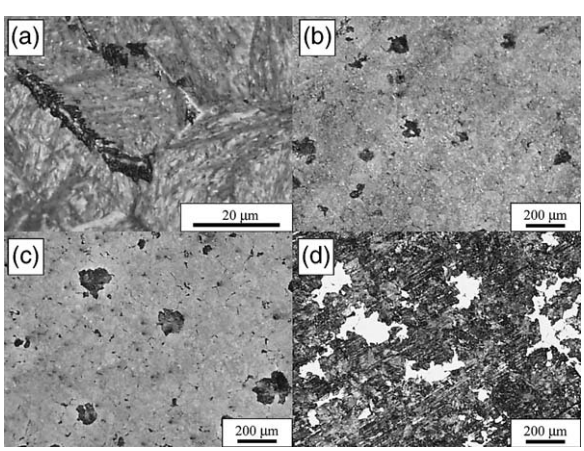

Fig. 1. Optical microscopy images of the microstructure at different stages of the isothermal austenite/pearlite phase transformation at $T = 953$ K. The samples were quenched to room temperature after 50 s (a), 100 s (b), 150 s (c), and 200 s (d). Note that the magnification for (a) is 20× larger than for (b), (c), and (d).

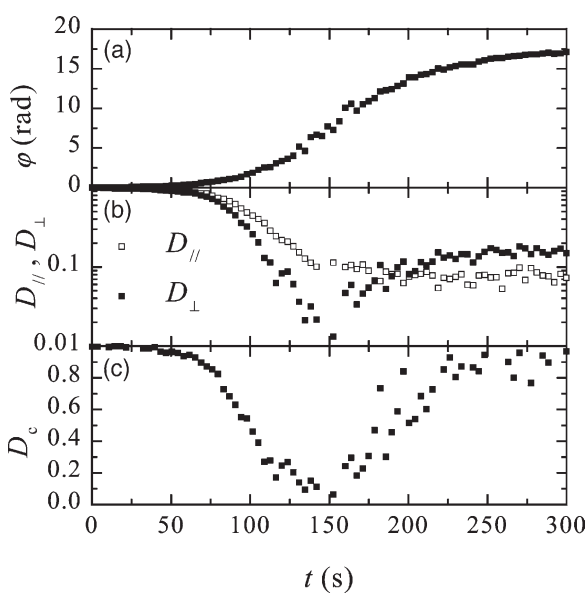

Fig. 2. The measured rotation of the polarization vector φ (a), the components of the depolarization matrix $\boldsymbol{D}$ parallel ($D_{//}$) and perpendicular ($D_{\perp}$) to the applied magnetic field (b), and the correction factor D_c (c) as a function of time t during the isothermal transformation at $T = 953$ K.

structure evolves from a random to a non-random distribution of pearlite colonies. For higher fractions D_c increases and finally reaches unity at the end of the transformation. This indicates that the pearlite clusters start to form an interconnected network resulting in a more homogeneous structure. This behavior corresponds to the evolution of the microstructure as shown in Fig. 1.

Fig. 3 shows the formed fraction f and average magnetic particle radius δ which were determined from 3DND measurements as a function of time for the three isothermal transformations. The deduced average magnetic domain size is corrected for the extra depolarization, which is caused by a non-random distribution of magnetic domains. A largely depolarized neutron beam (see Fig. 2(b)) causes the large error bars, which appear in the region half way the transformation. The increase in average particle size between $f = 0.1$ and 0.5 in Fig. 3(b) represents to the average pearlite growth rate G, which is given in Table 1.

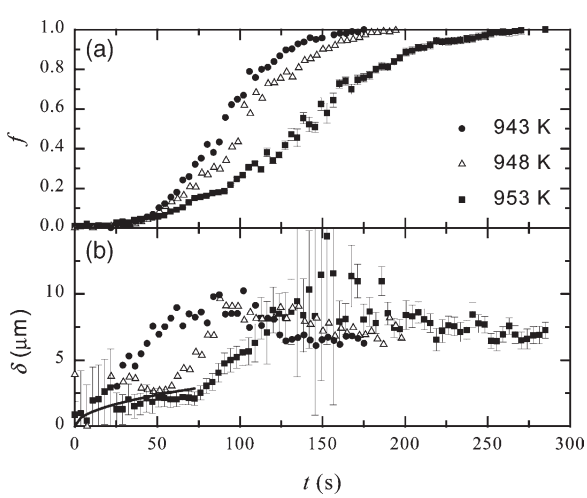

Fig. 3. The fraction pearlite f (a) and average magnetic particle radius δ (b) as a function of time for isothermal transformations at 943 K (solid sphere), 948 K (open triangle), and 953 K (solid square). For clarity reasons only the error bars at 953 K are shown. Comparable errors are observed for the other two temperatures. The solid line represents the Zener theory for the formation of pro-eutectoid ferrite.

6. Discussion

At a moderate undercooling the austenite/pearlite transformation in eutectoid steel is characterized by a non-random distribution of pearlite colonies during the transformation. The optical microscopy and 3DND measurements show that a first small amount of pro-eutectoid ferrite is formed. The pearlite colonies randomly nucleate at the formed pro-eutectoid ferrite grains and austenite grain corners just after the steel started to transform. Shortly thereafter, new pearlite colonies nucleate next to the existing pearlite colonies. At this stage large clusters of pearlite colonies are formed. However, new pearlite colonies also nucleate at austenite grain boundaries, which results in a mixture of individual pearlite colonies and clusters of pearlite colonies. At this stage there are a few clusters of pearlite colonies, which are very large (≈160 μm) and many relatively small individual pearlite colonies (≈15 μm), as indicated in Fig. 1. Towards the end of the transformation, the clusters start to impinge until all pearlite colonies are connected and a homogeneous structure is formed at the end of the transformation.

The increase in average particle size during the first 75 s of the transformation at $T = 953$ K (see Fig. 3(b)) corresponds to the growth of pro-eutectoid ferrite, of which the radius R^α increases as a function of time according to the Zener-theory (solid line in Fig. 3(b)) [31]. The analytical results can be approximated by the following relation:

$$R^\alpha = 2.102\left(\frac{C^\gamma_\infty - C^\gamma_{eq}}{C^\alpha_{eq} - C^\gamma_\infty}\right)^{0.5871}\sqrt{D^\gamma_c t}, \qquad (18)$$

where C^γ_{eq}(≈0.77 wt.%) and C^α_{eq}(≈0.02 wt.%) are the equilibrium carbon concentrations in the austenite and ferrite, respectively. C^γ_∞ is the carbon concentration in the austenite matrix away from the interface. In the present case C^γ_∞ is assumed to be equal to the average carbon concentration (0.715 wt.%). The average carbon concentration in the remaining austenite will hardly change throughout the transformation, because this is a nearly eutectoid steel. With increasing undercooling the pro-eutectoid ferrite has less time to grow and less pro-eutectoid ferrite will form.

Table 1
Thermodynamic and kinetic parameters of the studied nearly eutectoid steel for the three isothermal transformation temperatures. ΔT is the undercooling. Δg_V^θ is the driving force for cementile nucleation, k_n is a temperature dependent prefactor that is related to the time dependent nucleation rate. G is the measured pearlite growth rate. $t_{1/2}$ is the time to transform half of the volume. n is the Avrami exponent

T (K)	ΔT (K)	Δg_V^θ (J/mol)	k_n ($mm^{-3}s^{-2}$)	G (μm/s)	$t_{1/2}$ (s)	n
943	52	−1613	61(3)	0.15(2)	88(1)	3.31(7)
948	47	−1486	31(2)	0.14(1)	101(1)	3.14(8)
953	42	−1359	16(1)	0.119(5)	135(1)	2.77(4)

6.1. Nucleation

The fraction f of the phases formed can be expressed as

$$f = \frac{4}{3}\pi\delta_\alpha^3 N_\alpha + \frac{4}{3}\pi\delta_p^3 N_p \tag{19}$$

where δ_α and δ_p are the average pro-eutectoid ferrite grain and pearlite colony radius, respectively. N_α and N_p represent the number of pro-eutectoid ferrite grains and pearlite colonies, respectively. From Eq. (19) the number of pearlite nuclei N_p can be estimated as a function of transformation time t, which is shown in Fig. 4 for the three isothermal transformations. The number of pearlite nuclei is found to increase quadratically with time. In literature it is reported that the number of pearlite nuclei scales with the third power of time [32–34].

The measured number of pearlite colonies N_p can be compared to the classical nucleation theory, after integration of Eq. (1) with respect to time. The integrated equation that gives the number of pearlite colonies as a function of time can be approximated by

$$N_p = k_n t^2 \tag{20a}$$

for times between $t = 0$ and 2τ, with

$$k_n \propto \exp\left(-\frac{\Psi}{\Delta g_V^2 k_B T}\right). \tag{20b}$$

The fact that the number of pearlite nuclei increases quadratically with time, as we have observed, means that the pearlite transformation is finished before the steady state nucleation rate is reached. The lines in Fig. 4 represent the fits to Eqs. (20a) and (20b), which resulted in the values for k_n that are given in Table 1.

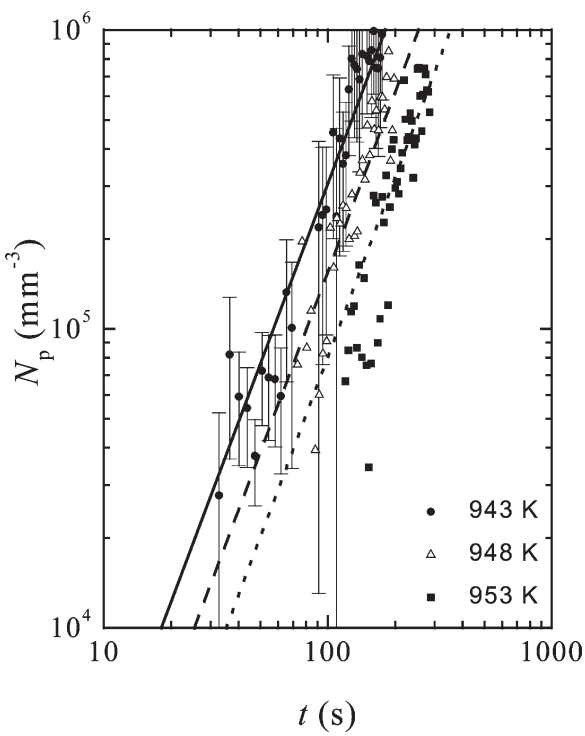

Fig. 4. The number of pearlite colonies N_p as a function of the transformation time t for the isothermal transformations at 943 K (solid sphere, straight line), 948 K (open triangle, dashed line), and 953 K (solid square, dotted line).

The rate controlling mechanism for the nucleation of pearlite in hypo-eutectoid steels is the nucleation of cementite, since the pro-eutectoid ferrite continues to grow into the pearlite [6]. The driving force for cementite nucleation Δg_V^θ is cal-

culated for the binary Fe-C system from the thermodynamic database MTDATA®. The common tangent along the ferrite and austenite Gibbs free energy curves was constructed to calculate Δg_V^θ, which means that it is assumed that the ferrite and austenite are in equilibrium before the cementite nucleates. The values for Δg_V^θ are given in Table 1. A best fit of $\ln(k_n)$ to $-[(\Delta g_V^\theta)^2 k_B T]^{-1}$ gives a value of $\Psi_\theta = 2.2(2) \times 10^{-3}$ J^3/m^6 for cementite nucleation during the pearlite formation.

The activation energy for nucleation is directly proportional to the factor Ψ, as can be seen from Eq. (2). If for example the energy that is required for the formation of a new interface is almost balanced by the energy that is released by transformation, nucleation can take place relatively easily, because the activation energy is then relatively small. From in-situ synchrotron measurements it was recently determined that for the austenite/ferrite phase transformation in medium carbon steel $\Psi_\alpha = 5\times10^{-8}$ J^3/m^6 for the nucleation of ferrite [1]. A comparison between Ψ_α and Ψ_θ shows that the effect of interfacial energies on the activation energy for the cementite nucleation during the pearlite formation is approximately 10^5 times higher than for the ferrite nucleation. This is probably related to the fact that during the nucleation of pro-eutectoid ferrite high-energy austenite/austenite grain boundaries are replaced by mainly low-energy or almost coherent austenite/ferrite interfaces. The pro-eutectoid ferrite continues to grow with the same crystallographic orientation during the pearlite formation as part of a pearlite colony [1]. This means that cementite nucleation forms the rate-limiting step during pearlite nucleation. During the cementite nucleation, all the energy that is released by the removal of the low-energy austenite/ferrite interface is probably used for the formation of the low-energy ferrite/cementite interface. There is not enough energy left to compensate the energy that is necessary for the formation of the austenite/cementite interface. The main difference between the nucleation of pro-eutectoid ferrite and pearlitic cementite is that the former takes place at high-energy grain boundaries, while the latter takes place at low-energy interfaces. This difference results in a relatively high value for Ψ_θ compared to Ψ_α, which means that the nucleation of pro-eutectoid ferrite is relatively easy compared to the nucleation of pearlitic cementite.

The relatively high value for Ψ_θ may explain the general observation (see e.g. [1]) that during continuous cooling the formation of ferrite may take place at exactly the equilibrium transition temperature, while the subsequent formation of pearlite takes place below its equilibrium transition temperature. In order to form a cementite nucleus during the pearlite formation, Δg_V^2 needs to increase to compensate for the large value of Ψ_θ. As Δg_V^2 increases with increasing undercooling, the temperature at which pearlitic cementite forms is distinctly below the equilibrium transition temperature.

6.2. Pearlite growth

The average growth rate of the pearlite colonies was only measured during the first half of the transformation. The measured average growth rate at 953 K is $G = 0.12$ μm/s, which is approximately a factor 8 smaller than the value found from a series of quenched specimens of an Fe-0.8C–0.6Mn alloy at 963 K [33]. This difference is possibly caused by the fact that the quench-method gives an estimate of the highest measured pearlite growth rate rather than the average growth rate, given by the 3DND method.

In order to determine the rate-controlling mechanism for the growth of pearlite, $\ln(G/D^\gamma_{C,V})$ and $\ln(G/D^\gamma_{C,GB})$ are plotted as a function of the undercooling ΔT in Fig. 5. The measured average pearlite growth rate G is either scaled by the volume or grain boundary diffusion coefficient of the carbon atoms. The transition temperature was estimated from MTDATA® to be $T_{A1} = 995$ K. The solid line in Fig. 5(a) represents a fit of the data to Eq. (8) with the volume diffusion coefficient of carbon ($D^\gamma_{C,V}$) and $\beta = 2$. A best fit of the data in Fig. 5(a) to Eq. (8) gives a slope of $\beta = 2.1(3)$, which is consistent with the theoretical prediction of $\beta = 2$ for volume diffusion of carbon.

Fig. 5(b) shows the same data points as in Fig. 5(a), but scaled by the grain boundary diffusion coefficient of the carbon atoms $D^\gamma_{C,GB}$. The solid line in Fig. 5(b) represents a fit to Eq. (8) with the

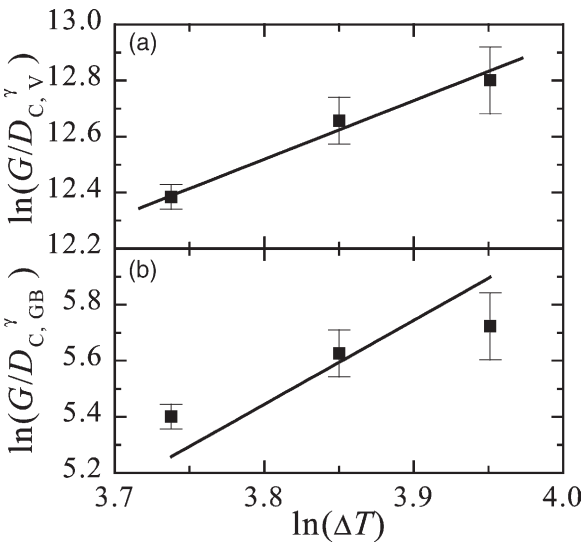

Fig. 5. The average growth rate of the pearlite colonies, which was scaled by the temperature dependent volume diffusion coefficient of the carbon atoms $\ln(G/D_{C,V}^{\gamma})$ (a) and by the grain boundary diffusion coefficient of the carbon atoms $\ln(G/D_{C,GB}^{\gamma})$ (b) as a function of the undercooling $\ln(\Delta T)$. The solid lines represent the theory that volume diffusion ($\beta = 2$) (a) or grain boundary diffusion ($\beta = 3$) (b) is the rate-controlling mechanism for pearlite growth.

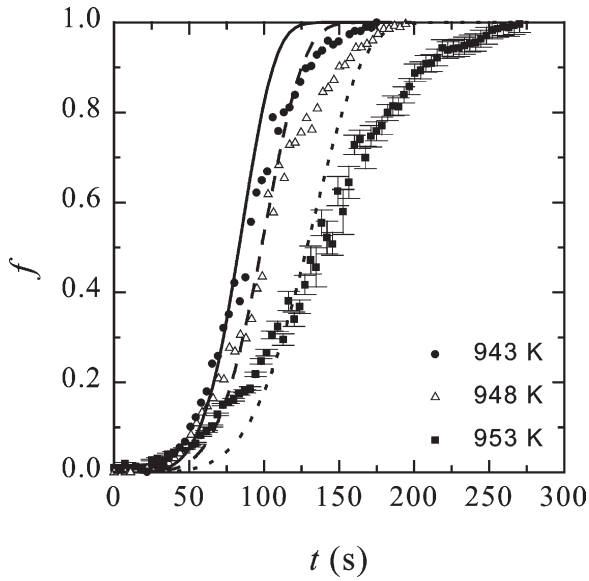

Fig. 6. Comparison between the measured and calculated formed fraction as a function of the transformation time for the isothermal transformations at 943 K (solid sphere, straight line), 948 K (open triangle, dashed line), and 953 K (solid square, dotted line).

grain boundary diffusion coefficient ($D_{C,GB}^{\gamma}$) and the theoretical value $\beta = 3$. A best fit of the data in Fig. 5(b) with Eq. (8) gives $\beta = 1.7(3)$, indicating a large discrepancy with the theoretical prediction. This means that volume diffusion of the carbon atoms is the rate-controlling mechanism for the pearlite growth at temperatures that are relatively close to the transition temperature. However, in the case that site saturation of the available pearlite nucleation sites takes place on the former austenite grain boundaries, grain boundary diffusion of the carbon atoms can be the rate-controlling mechanism for pearlite growth.

6.3. Overall transformation

Fig. 6 shows a comparison between the measured and the calculated formed fraction as a function of the transformation time for the three isothermal transformation temperatures. The experimental data can be fitted to a generalized KJMA equation

$$f(t) = 1-\exp(-kt^n), \tag{21}$$

where $k = \ln(2)(t_{1/2})^{-n}$ is a rate constant and n is referred to as the Avrami exponent. The time to transform half of the volume is represented by $t_{1/2}$. A best fit of the experimentally observed fraction curves of Fig. 6 with the generalized KJMA equation shows that $n \approx 3$ (see Table 1).

The lines in Fig. 6 represent the fractions formed, which were calculated by inserting the observed nucleation rate $\dot{N}_p$ and growth rate G_V in Eq. (11). The experimental nucleation rate $\dot{N}_p$ is, however, normalized to the sample volume instead of the untransformed volume. We can write

$$\dot{N}_u = \frac{\dot{N}_p}{1-f} \approx \dot{N}_p. \tag{22}$$

for small fractions of pearlite. Note that the classical nucleation theory in the form of Eqs. (20a) and (20b) is the same as Eq. (10) after integration with respect to time with $m = 1$.

From Fig. 4 we found that the number of pearlite colonies increases quadratically with time, which means that $m = 1$, and from Fig. 3 we found that

the growth rate is approximately constant. If we assume that the growth is radial ($d = 3$), the Avrami exponent becomes $n = d + m + 1 = 5$. From Fig. 6 it is apparent that the calculated fraction curve deviates from the experimental observation ($n \approx 3$).

A likely explanation for the difference between the calculated fraction curve and the experimental observation is the following. At the start, the transformation proceeds faster than predicted from Eq. (11) with $n = 5$, because of the formation of pro-eutectoid ferrite. At the end, the transformation proceeds slower than predicted, which is expected to be due to the non-random distribution of nuclei. In that case the growing colonies impinge at an earlier stage than if the nuclei were randomly distributed, which reduces the overall transformation rate. Furthermore, the average pearlite growth rate at the end of the transformation can be different than that measured during the first half of the transformation and Eq. (22) no longer holds for large fractions. Although, the experimentally observed nucleation and growth rates are used in the calculation of the fraction transformed from the KJMA theory, the comparison with experimentally observed fraction transformed shows once more that the KJMA theory does not give an exact prediction unless its restrictive assumptions are completely fulfilled [35].

7. Conclusions

Three-dimensional neutron depolarization and optical microscopy measurements were performed in order to study the evolution of the microstructure during the austenite/pearlite transformation in a nearly eutectoid steel. At temperatures that are relatively close to the transition temperature, the transformation is characterized by a non-random distribution of pearlite colonies. The in-situ measurements show that the pearlite nucleation rate is a transient nucleation process, which can be described by the classical nucleation theory. The number of pearlite colonies increases quadratically with time. We find that the effect of interfacial energies on the activation energy for cementite nucleation during the pearlite formation is approximately 10^5 times higher than for the nucleation of pro-eutectoid ferrite. The average pearlite growth rate, which was measured in-situ during the first half of the transformation, corresponds to the theoretical prediction for volume diffusion as the rate-controlling mechanism for the growth of pearlite. A KJMA type of model, which includes the measured nucleation and growth rates deviates from the measured overall transformation rate, because of the presence of pro-eutectoid ferrite and a non-random distribution of pearlite colonies.

Acknowledgements

We thank N. Geerlofs for performing the quench experiments. This work was financially supported in part by the Netherlands Foundation for Technical Sciences (STW) of the Netherlands Organisation for Scientific Research (NWO).

References

[1] Offerman SE, Van Dijk NH, Sietsma J, Grigull S, Lauridsen EM, Margulies L, Poulsen HF, Rekveldt MTh, Van der Zwaag S. Science 2002;298:1003–1005.
[2] Thompson SW, Howell PR. Scripta Metall 1988;22:1775–1778.
[3] Zener C. Trans AIME 1945;167:550–595.
[4] Hillert M. Jerkont Ann 1957;141:757–789.
[5] Hillert M. Met Trans 1972;3:2729–2741.
[6] Frye JH, Stansbury EE, McElroy DL. Trans AIME 1953;197:219.
[7] Cheetman D, Ridley N. J Iron Steel Inst 1973;211:648–652.
[8] Pearson DD, Verhoeven JD. Metall Trans A 1984;15A:1037–1045.
[9] Ridley N. In: Phase transformations in ferrous alloys. Warrendale, PA: TMS-AIME; 1984.
[10] Sundquist BE. Acta Metall 1968;16:1413–1427.
[11] Whiting MJ. Scipta Mater 2000;43:969–975.
[12] Kolmogorov AN. Izv Acad Nauk SSSR, Ser Materm 1937;3:355–359.
[13] Johnson J, Mehl R. Trans AIME 1939;135:416–442.
[14] Avrami M. J Chem Phys 1939;7:1103–1112.
[15] Avrami M. J Chem Phys 1940;8:212–224.
[16] Avrami M. J Chem Phys 1941;9:117–184.
[17] Rekveldt MTh. Z Phys 1973;259:391–410.
[18] Rosman R, Rekveldt MTh. J Magn Magn Mater 1991;95:319–340.
[19] Te Velthuis SGE, Van Dijk NH, Rekveldt MTh, Sietsma J, Van der Zwaag S. Acta Mater 2000;48:1105–1114.
[20] Van Wilderen LJGW, Offerman SE, Van Dijk NH,

Rekveldt MTh, Sietsma J, Van der Zwaag S. Appl Phys A 2002;74;1052–1054.
[21] Offerman, SE, Van Wilderen LJGW, Van Dijk NH, Rekveldt MTh, Sietsma J, Van der Zwaag S. Physica B, (in press)
[22] Aaronson HI, Lee JK. In: Lectures on the theory of transformations. Warrendale, PA: TMS-AIME; 1975.
[23] Jena AK, Chaturvedi MC. Phase transformations in materials. London: Prentice-Hall, 1992.
[24] Ågren J. Scripta Metall 1986;20:1507–1510.
[25] Porter DA, Easterling KE. Phase transformations in metals and alloys. London: Chapman & Hall, 1993.
[26] Howell PR. Mat Char 1998;40: 227–260.
[27] Cahn JW. Trans AIME 1957;209:140–144.
[28] Van Dijk, NH, Te Velthuis SGE, Rekveldt MTh, Sietsma J, Van der Zwaag S. Physica B 1999;267–268:88–91.
[29] Arrott AS, Heinrich B. J Appl Phys 1981;52:2113–2115.
[30] Rosman R, Rekveldt MTh. Phys Rev B 1991;43:8437–8449.
[31] Zener C. J Appl Phys 1949;20:950–953.
[32] Scheil E, Langeweise A. Arch Eisenhttenw 1937;11:93.
[33] Hull FC, Colton RA, Mehl RF. Trans AIME 1942;150:185–207.
[34] Cahn JW, Hagel WC. In: Zackay VF, Aaronson HI, editors. Decomposition of austenite by Diffusional processes. New York: Interscience; 1962.
[35] Cahn JW. Mat Res Soc Proc 1996;398:425–437.